LETTERS

Genetic evidence that FGFs have an instructive role in limb proximal–distal patterning

Francesca V. Mariani[1]*†, Christina P. Ahn[1]* & Gail R. Martin[1]

Half a century ago, the apical ectodermal ridge (AER) at the distal tip of the tetrapod limb bud was shown to produce signals necessary for development along the proximal–distal (P–D) axis, but how these signals influence limb patterning is still much debated[1,2]. Fibroblast growth factor (FGF) gene family members are key AER-derived signals[3,4], with *Fgf4*, *Fgf8*, *Fgf9* and *Fgf17* expressed specifically in the mouse AER[5]. Here we demonstrate that mouse limbs lacking *Fgf4, Fgf9* and *Fgf17* have normal skeletal pattern, indicating that *Fgf8* is sufficient among AER-FGFs to sustain normal limb formation. Inactivation of *Fgf8* alone causes a mild skeletal phenotype[6,7]; however, when we also removed different combinations of the other AER-FGF genes, we obtained unexpected skeletal phenotypes of increasing severity, reflecting the contribution that each FGF can make to the total AER-FGF signal. Analysis of the compound mutant limb buds revealed that, in addition to sustaining cell survival, AER-FGFs regulate P–D-patterning gene expression during early limb bud development, providing genetic evidence that AER-FGFs function to specify a distal domain and challenging the long-standing hypothesis that AER-FGF signalling is permissive rather than instructive for limb patterning. We discuss how a two-signal model for P–D patterning can be integrated with the concept of early specification to explain the genetic data presented here.

Fgf8 is expressed in prospective AER cells of the nascent limb bud and, subsequently, throughout the AER until it regresses[8]. By contrast, *Fgf4*, *Fgf9* and *Fgf17* expression commences after the AER is formed, is restricted to the posterior AER, and ceases at least a day before AER regression[5] (Fig. 1a). When AER-FGFs are individually eliminated, only loss of *Fgf8* function perturbs skeletal patterning[5–7,9–11]. The other AER-FGFs have been proposed to be essential, but functionally redundant, components of a positive-feedback loop between the AER and the patterning centre in posterior limb bud mesenchyme that produces sonic hedgehog (SHH)[5,12,13]. We tested this hypothesis by deleting *Fgf4* by means of Cre-mediated recombination in the AER of embryos homozygous for *Fgf9* and *Fgf17* null alleles[10,11] (hereafter referred to as F4;9,17-triple knockout (TKO) mutants; Fig. 1b). Because *Fgf4* deletion occurs before *Fgf4* expression normally commences[5] (see Fig. 1a), the F4;9,17-TKO limb buds do not produce FGF4, FGF9 or FGF17. Nevertheless, in F4;9,17-TKO skeletons ($n = 6$), the three classically defined limb segments—stylopod (upper arm or leg), zeugopod (lower arm or leg) and autopod (wrist/hand or ankle/foot)—were essentially normally patterned (Fig. 1c). Consistent with this observation, *in situ* hybridization (not shown) and quantitative PCR after reverse transcription (qRT–PCR; Fig. 1d) showed normal *Shh* expression in F4;9,17-TKO limb buds at embryonic day (E)10.5. Moreover, there was no compensatory upregulation of *Fgf8* in F4;9,17-TKO limb buds at E10.5 (Fig. 1d). These data demonstrate that *Fgf8* is sufficient for normal limb development, including sustaining *Shh* expression, and that whatever positive regulatory interactions occur between *Shh* and the posterior AER-FGF genes, they are dispensable for normal limb skeletal development.

Although not required when FGF8 is present, each posterior AER-FGF (FGF4, FGF9 and FGF17) may contribute to limb development. Such contributions can be uncovered by inactivating these genes, singly or in combination, along with *Fgf8* (refs 14 and 15). To produce such double-knockout (DKO) and TKO mutants, we used *Msx2-cre*, which functions earlier in hindlimb than in forelimb buds[5] (see Fig. 1a). When inactivated by *Msx2-cre*, *Fgf8* is never expressed in hindlimb buds, but is transiently expressed in forelimb buds before E9.5; consequently, *Fgf8* knockout (F8-KO) hindlimbs are more severely affected than forelimbs[6]. In F8;4-DKO mutants, the hindlimb skeleton fails to form, whereas the forelimb skeleton develops but lacks many elements[14]. Likewise, in F8;4-DKO mutants lacking a copy of *Fgf9* (F8;4-DKO;F9$^{-/+}$ mutants), there was no hindlimb, but a more severely affected forelimb developed (see below). Compound mutant forelimbs thus provided a greater range of phenotypes for analysis than hindlimbs.

These forelimb phenotypes (summarized in Supplementary Table 1) could be ranked in order of increasing severity. F8-KO ($n = 10$), F8;17-DKO ($n = 8$) and F8-KO;F9$^{-/+}$ ($n = 6$) mutants displayed a similar mild phenotype, with all skeletal elements present except for one digit, and slight hypoplasia of the stylopod and zeugopod (Fig. 2a, b; data not shown; ref. 6). Similar defects were seen in F8;9-DKO ($n = 16$) and F8;9,17-TKO ($n = 8$) mutants, but the zeugopod posterior element (ulna) was short and the anterior element (radius) was absent (Fig. 2c; data not shown). The hindlimb zeugopod was similarly affected in these mutants, but, notably, it was the posterior zeugopod element (fibula) that was missing (not shown). Assays for *Sox9* expression, which marks the condensations that develop into skeletal elements[16], showed that these patterning defects were detectable by E12.5 (Fig. 2h–j; data not shown), demonstrating that AER-FGFs are essential for establishing skeletal pattern at limb bud stages. A more severe phenotype was observed in F8;4-DKO mutants ($n = 5$), in which the forelimb zeugopod consisted of only a hypoplastic ulna and all autopod elements were absent except for one or two phalanges (Fig. 2d; ref. 14). Removing one copy of *Fgf9* further increased phenotype severity ($n = 14$ mutants; Fig. 2e, f); when both copies were removed, F8;4;9-TKO mutants ($n = 9$) lacked all forelimb skeletal elements (Fig. 2g).

The simplest explanation for these data is that the individual AER-FGFs are functionally equivalent[17] but that they differ in the extent to which they contribute to the AER-FGF signal, presumably reflecting differences in their temporal and spatial expression profiles, levels of expression, and binding specificities to FGF receptors in the limb bud mesenchyme. If so, then the range of skeletal phenotypes observed

[1]Department of Anatomy and Program in Developmental Biology, School of Medicine, University of California at San Francisco, San Francisco, California 94158-2324, USA. †Present address: Broad Center for Stem Cell Research and Regenerative Medicine, Keck School of Medicine, University of Southern California, Los Angeles, California 90033, USA.
*These authors contributed equally to this work.

when specific combinations of AER-FGFs are removed reflects a change in the level of total AER-FGF signal. In support of this hypothesis, we found that at E10.5 the size and intensity of the expression domain of *Dusp6* (a downstream target of AER-FGF signalling[18]) negatively correlated with the severity of the mutant phenotype (Fig. 2l–o). Together, these data suggest that *Fgf8* makes the greatest contribution to the AER-FGF signal, followed by *Fgf4*, *Fgf9* and *Fgf17*. Furthermore, our data suggest that there is a critical threshold of AER-FGF signalling, below which skeletal elements do not form.

The phenotype of the F8;4-DKO;F9$^{-/+}$ forelimbs was especially notable: the stylopod (humerus) was present, but was often smaller than normal and truncated distally, with elements of a single digit immediately distal to it. The most distal element usually had the pointed tip of a terminal phalanx, occasionally with a nail overlying it (Fig. 2e, f; data not shown). Sometimes there was a substantial gap between the humerus and the phalangeal elements (Fig. 2f and Supplementary Table 1). The complete absence of the zeugopod and most of the autopod was confirmed by *Sox9* expression assays at E12.5 (Fig. 2k; see Supplementary Fig. 1 for data on *Hoxa11* expression). One possible explanation for this phenotype is that the severe reduction in AER-FGF signalling causes the death of most autopod and zeugopod progenitors in the early limb bud. However, consistent with previous reports[14,15], mesenchymal cell death in F8;4-DKO;F9$^{-/+}$ mutants was detected in a proximal dorsal region at E10.5, and not distally (Fig. 3c), where autopod and distal zeugopod progenitors reside[19]. Cell death remained proximally restricted until E11.5, after which it was no longer detected (not shown). In mutant limb buds with more AER-FGF signalling, the cell death domain occupied a smaller percentage of limb bud volume (Fig. 3a–d; data not shown). Because the dying cells are proximally localized, it seems unlikely that autopod or zeugopod progenitor cell death is the main cause of the phenotype.

Another possible explanation for the lack of zeugopod and most of the autopod in F8;4-DKO;F9$^{-/+}$ forelimbs, is that AER-FGFs are involved in specifying distal cell fate, and when AER-FGF signalling is markedly reduced, fewer cells are specified as distal. This hypothesis could be tested by examining the effects of reducing AER-FGF signalling on the expression of genes essential for P–D specification. *Meis1*, which encodes a homeobox transcription factor, is potentially one such gene because ectopic *Meis1* expression is reported to induce distal-to-proximal transformations in chicken limb buds[20]. Initially, *Meis1* expression is detected throughout the nascent limb bud mesenchyme; subsequently, a *Meis1*-negative distal domain is established and increases in size as the limb bud expands[20]. Consistent with a role for FGFs in specification of a distal domain, FGF-bead implantation and drug inhibition studies showed that FGF signalling can repress *Meis1* expression[21]. Moreover, we previously found that the extent of the *Meis1*-negative expression domain was reduced in

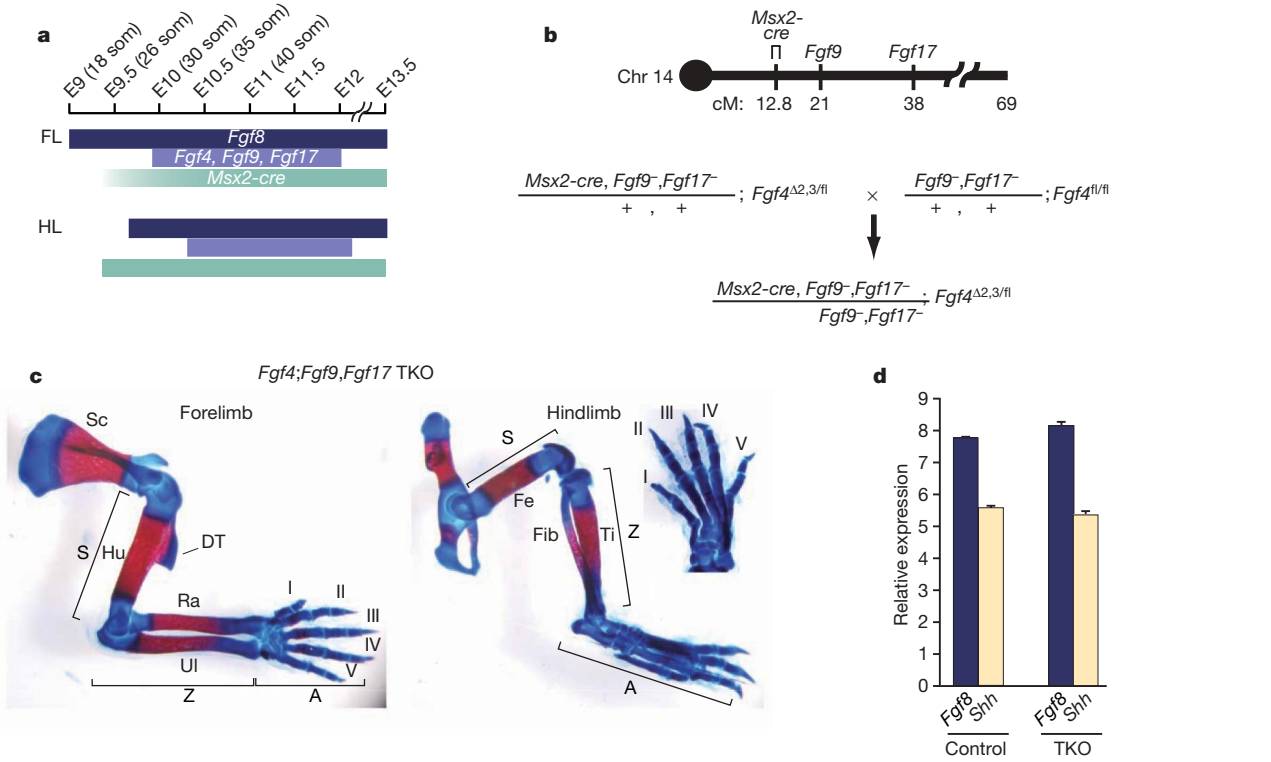

Figure 1 | *Fgf8* is sufficient for normal limb development. **a**, Schematic diagram illustrating temporal aspects of wild-type AER-FGF gene expression and the stages at which the *Msx2-cre* transgene functions to inactivate the *Fgf8* and *Fgf4* floxed alleles in the AER. Note that development of forelimb (FL) buds, as marked by *Fgf8* expression, commences before that of hindlimb (HL) buds, that *Fgf8* expression precedes that of *Fgf4*, *Fgf9* and *Fgf17*, and that *Msx2-cre* functions earlier in hindlimb than in forelimb buds[5,6]. **b**, Schematic diagram of mouse chromosome 14, showing the map positions of *Fgf9*, *Fgf17* and the *Msx2-cre* transgene, which lies within 1 centimorgan (cM) of *Bmpr1a* (not illustrated) and 12.8 cM from the centromere (circle)[28]. Because of this linkage, once the parental animals (male on left; female on right) were generated we could produce progeny of the genotype illustrated (*Fgf4*;*Fgf9*,*Fgf17* TKO mutants), in which the *Fgf4* conditional null allele (*Fgf4*^{fl}) is converted by *Msx2-cre* function in the AER to *Fgf4*$^{\Delta 2,3}$, a null allele lacking exons 2 and 3, at a frequency of 12.5% ($n = 6/48$), close to the expected frequency of 15.5%. **c**, *Fgf4*;*Fgf9*,*Fgf17* TKO forelimb and hindlimb skeletons at E17.5; these are indistinguishable from those of the wild type (not shown), except for an enlarged deltoid tuberosity caused by loss of *Fgf9* function after condensation[29]. **d**, Quantitative RT–PCR assays for *Fgf8* and *Shh* expression. A representative experiment on forelimb buds from embryos at ~E11.0 (39–40 somites; $n = 4$ limb buds for each genotype) is shown. Values are normalized to cyclophilin expression and are shown as means ± standard deviation. The difference between control and mutant limb buds with respect to *Fgf8* and *Shh* expression was not significant (*Fgf8*, $P = 0.61$; *Shh*, $P = 0.80$). A two-tailed Student's *t*-test was employed, using the average of triplicate cycle count values for each limb bud. Similar results were obtained for limb buds at 33, 34, 35 and 37 somites. Abbreviations: A, autopod; DT, deltoid tuberosity; Fe, femur; Fib, fibula; Hu, humerus; Ra, radius; Sc, scapula; S, stylopod; som, somite number; Ti, tibia; Ul, ulna; Z, zeugopod; I–V, digit numbers from anterior to posterior.

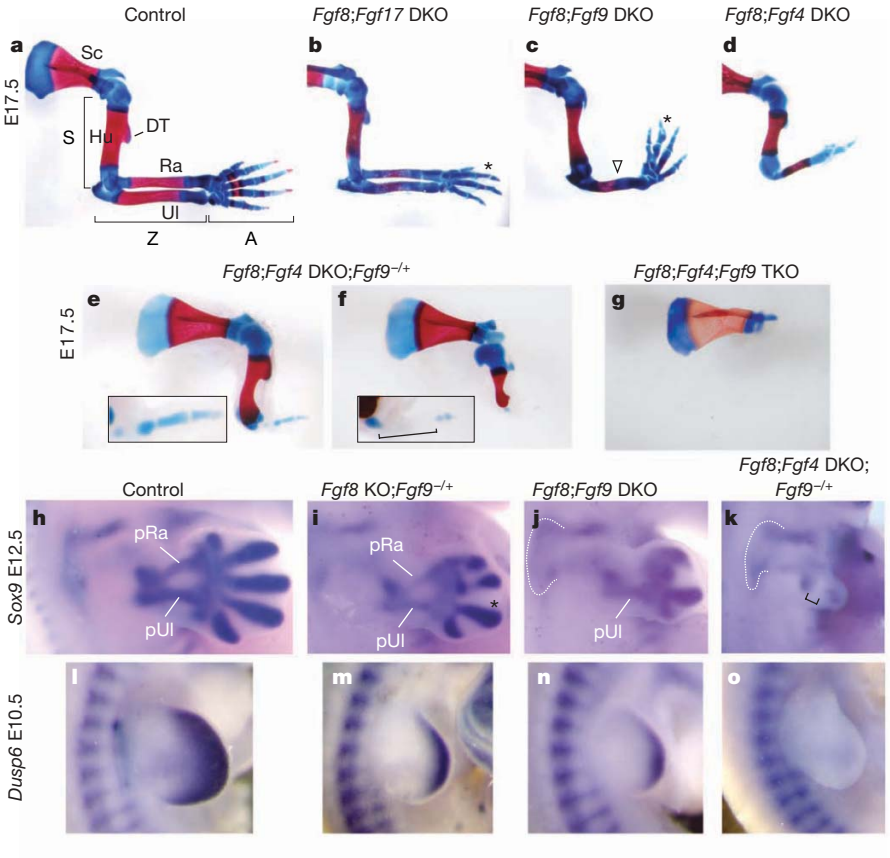

Figure 2 | Effects of inactivating AER-FGF genes on skeletal development. **a**–**g**, Comparison of skeletal preparations of forelimbs from E17.5 embryos of the genotypes indicated. The asterisk in **b**, **c** and **i** indicates that the mutant autopod has only four digits. The open down-triangle (**c**) indicates the lack of the anterior element (radius). The differences in humerus thickness/shape and deltoid tuberosity size among mutants of the various genotypes illustrated in **b**–**d** were also observed among mutants of the individual genotypes, suggesting they are caused by background genes. **e**, **f**, Two examples of *Fgf8*;*Fgf4*-DKO;*Fgf9*$^{-/+}$ forelimb skeletons, illustrating the more (**e**) and less (**f**) common phenotypes, respectively. The insets show the distal element of the limbs at higher magnification. The bracket (**f**) indicates the gap between the distal end of the humerus and the digit-like element. **h**–**o**, Expression of *Sox9* at E12.5 and of *Dusp6* at E10.5 (37 somites), as detected by RNA *in situ* hybridization in whole-mount in forelimb buds from embryos of the genotypes indicated. *Sox9* expression marks the condensations that prefigure the skeletal elements. The dotted white lines (**j** and **k**) outline the condensations that will develop into the scapula. Note the absence of the developing radius (**j**). The bracket (**k**) demarcates the region devoid of *Sox9*-positive cells between the developing condylar portion of the humerus and a distal condensation that presumably represents the distal part of a digit. pRa, prospective radius; pUl, prospective ulna. Other abbreviations are as in the legend to Fig. 1.

F8;F4-DKO limb buds[14]. However, because the F8;F4-DKO limb buds were considerably smaller than those of controls, it was impossible to know whether the observed effect was secondary to the reduction in limb bud size.

We were able to examine the effects of reducing AER-FGF signalling on *Meis1* expression independent of its effects on limb bud size, because the various AER-FGF compound mutant limb buds, although smaller than normal, were remarkably similar in overall size at E10.5 (Fig. 3e–h; data not shown). One explanation for this finding is that their size at E10.5 reflects the elimination of cells that died due to inactivation of *Fgf8*, which is expressed from ~E9.0 and inactivated by ~E9.5, whereas the effects of loss of *Fgf4* and *Fgf9* function on cell survival are not yet evident because their expression begins later than *Fgf8* expression. By E11.5, however, size differences became evident among the compound mutants; this was caused by extensive cell death and possibly a negative effect on cell proliferation after E10.5. These size differences were correlated with the decrease in AER-FGF signalling (not shown) and, subsequently, with skeletal phenotype severity (Fig. 2h–k and data not shown). Assays for *Meis1* at E10.5, when limb bud size was similar, showed that the *Meis1*-negative, distal domain was significantly reduced in F8;9-DKO and was further reduced in F8;4-DKO;F9$^{-/+}$ forelimb buds (Fig. 3i–l). To our knowledge, these data provide the first genetic evidence that AER-FGFs repress expression of a gene presumed to be involved in specification of proximal cell identity. In summary, we conclude that AER-FGF signalling serves at least two vital roles during limb development: to promote cell survival and to specify distal cell fate.

An important question is how our data fit with existing models for limb P–D patterning. The 'progress zone' model[22] postulates that the P–D pattern develops gradually, with cells in the distal limb bud mesoderm acquiring progressively more distal positional information over time, and that AER signals are not instructive for P–D patterning, but instead are 'permissive', keeping distal cells labile and able to change positional values by an unknown mechanism. However, our data showing that AER-FGF signalling is necessary to regulate *Meis1* expression indicate that it functions as an instructive rather than a permissive signal in limb development. Furthermore, the phenotypes of AER-FGF mutant skeletons (for example, F8;4-DKO;F9$^{-/+}$ forelimbs, which contain stylopod and autopod but no zeugopod elements) are not readily explicable by the progress zone model[1,14], which describes limb patterning as a progressive process whereby distal is specified only after proximal.

By contrast, the 'early specification' model[23] postulates that cells along the limb P–D axis are specified to form the stylopod, zeugopod and autopod limb segments at an early limb bud stage. Although not originally considered in this context, one model that can explain how such early specification occurs is the 'two-signal model'. This proposes that limb bud cells are initially exposed to a proximal signal

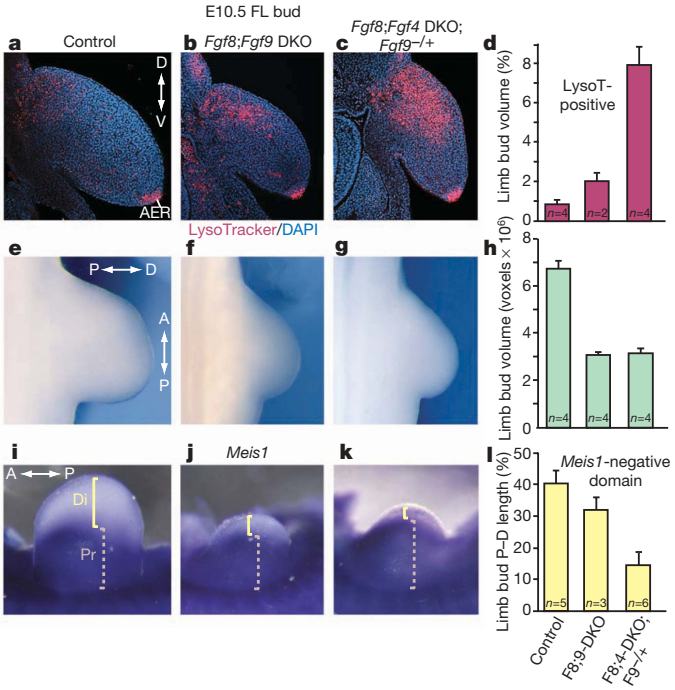

Figure 3 | Effects of inactivating AER-FGF genes on cell survival, limb bud size and *Meis1* expression. **a–c**, Confocal images of sections through E10.5 forelimb limb buds (35–36 somites) of the genotypes indicated stained with LysoTracker Red (which labels apoptotic cells as well as healthy cells engulfing apoptotic debris[30]) and DAPI (blue, which labels nuclei). **d**, Graph showing the average percentage of limb bud volume that is LysoTracker-Red-positive for each genotype. The difference between the two mutants was statistically significant ($P = 0.014$, two-tailed Student's *t*-test). **e–g**, Dorsal views of E10.5 forelimb buds (36–37 somites) from embryos of the genotypes indicated. **h**, Graph showing the average total volume of E10.5 limb buds (35–37 somites) of the genotypes indicated. No statistically significant difference was detected between mutants ($P = 0.79$, two-tailed Student's *t*-test). **i–k**, E10.5 forelimb buds (37 somites) were assayed in whole mount by RNA *in situ* hybridization for *Meis1* expression. The dashed tan and solid yellow brackets in each panel demarcate the *Meis1*-positive proximal and *Meis1*-negative distal domains in the limb bud mesenchyme, respectively. The length of each bracket reflects the average of the four measurements made on each sample. **l**, The average percentage of total limb bud proximal–distal (P–D) length (the sum of the lengths of the proximal and distal domains) that is *Meis1*-negative is shown for each limb bud. The difference between mutants was statistically significant ($P = 0.0003$, two-tailed Student's *t*-test). In **d**, **h** and **l**, *n* defines the number of limb buds analysed for each genotype, and the error bars show the standard deviation. Abbreviations: A↔P, anterior–posterior; AER, apical ectodermal ridge; D↔V, dorsal–ventral; *P*↔D, proximal–distal.

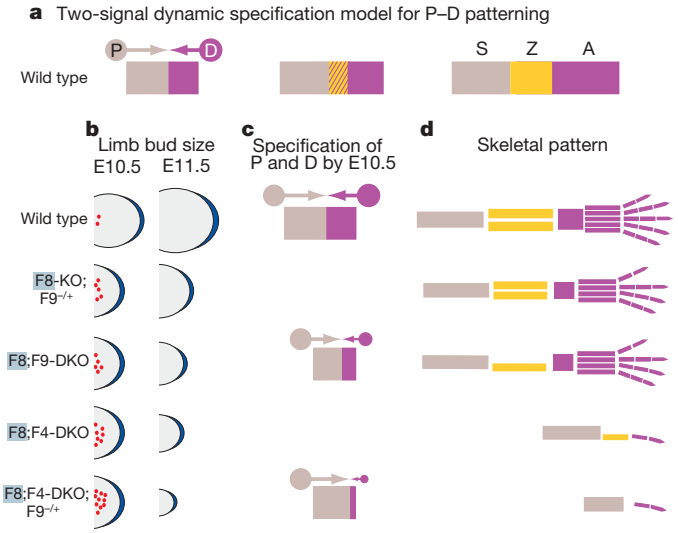

Figure 4 | AER-FGF mutant phenotypes can be explained by a two-signal dynamic specification model for limb proximal–distal patterning. **a**, Left, proximal (P) signal(s) from flanking mesoderm and opposing distal (D) signal(s) from the AER (FGFs) specify P (tan) and D (purple) domains[2,21] in the limb bud by E10.5; centre, a third, middle domain (cross-hatched) forms within the D domain, a hypothesis supported by recent fate mapping studies[19]; right, the three domains develop into the classically defined segments: stylopod (S, tan), zeugopod (Z, gold) and autopod (A, purple). **b**, Wild-type and AER-FGF mutant forelimb buds (dorsal views). At E10.5, all mutant limb buds are equal in size but are smaller than the wild type (quantified in this study for all genotypes except F8;4-DKO), and contain dying cells in the mesenchyme (red dots; cell death in AER not depicted). By E11.5, mutant limb bud size is decreased in proportion to the reduction in AER-FGF signal; dying cells are no longer observed in the mesenchyme. **c**, *Meis1*-positive P (tan) and *Meis1*-negative D (purple) domains are specified by opposing P and D signals, respectively. In the mutants, only the D signal is reduced, in proportion to the AER-FGF signal. Because the D signal is weaker than normal and also because the limb bud is smaller than normal due to cell death specifically in the P domain, the P signal extends over a region that, in wild-type limb buds, would normally be exposed to the D signal. **d**, Diagrams representing the size and number of elements in forelimbs of each genotype at birth. Owing to changes in the extent of limb bud P–D length influenced by P and D signals in the mutants at E10.5 (arrows in **c**), cells normally fated to form Z or A elements are specified as proximal and instead develop into S. For example, in F8;9-DKO limb buds, some Z and A elements are missing whereas S is nearly normal. In F8;4-DKO;F9$^{-/+}$ limb buds, all Z and all but the distal-most A elements are missing, whereas S forms but is reduced in size.

from mesoderm flanking the limb bud, possibly retinoic acid, and then to an opposing distal signal (FGF) from the AER, which establish proximal and distal domains, respectively[2,21]. Formation of a third (middle) domain might then occur as a result of interactions between cells at the boundary between proximal and distal domains over time, thus creating the three domains from which the stylopod, zeugopod and autopod segments will develop (see Fig. 4a). Additional domains within the autopod, from which wrist elements, metacarpals and digits develop, might likewise form as a result of cell–cell interactions at domain boundaries. This concept is consistent with the intercalation models proposed to explain amphibian limb regeneration[24,25]. Early specification would thus be a 'dynamic' process that takes place in concert with limb bud outgrowth. Our data support this model by providing genetic evidence that AER-FGFs function as an initial distal signal at early stages in limb development.

Such a two-signal dynamic specification model can easily explain the forelimb skeletal abnormalities reported here based on our findings that AER-FGFs have a dual function in limb development. Thus, we suggest that in the AER-FGF mutants, the distal signal is reduced in proportion to the decrease in AER-FGF signal. Because there is less opposing distal signal, the proximal signal, which is produced at the normal level, extends more distally than normal, specifying cells that would normally have formed distal elements to be proximal and thereby compromising autopod and zeugopod development. However, the stylopod is not abnormally long because proximal cells die in the AER-FGF mutants (Fig. 4b–d; see Supplementary Fig. 2a, b). This model of AER-FGF dual function can also explain the limb skeletal defects observed in other studies of mouse mutants[6,7,14] and X-irradiated chicken limb buds[26] in which the stylopod is severely reduced but distal elements are less affected (see Supplementary Fig. 2c).

Presently, it is not possible to assess when segment specification occurs and critical tests of this model cannot be performed because there are no molecular markers for the progenitors of the different segments. A promising avenue for identifying such markers has recently been opened by the demonstration that cells in proximal and distal regions of the early chicken limb bud are distinguishable

by their sorting behaviours *in vitro*[27]. It will be intriguing to determine whether FGFs produced in the AER are involved in establishing these differences.

METHODS SUMMARY

Production of mice. The mutant alleles used in this study were maintained on a mixed genetic background. F4;9,17-TKO mutants were generated by crossing parental animals of the genotypes depicted in Fig. 1b. Animals of the other genotypes were produced by generating and crossing appropriate parental mice. Control animals were offspring that did not inherit the *Msx2-cre* transgene.

Limb bud analysis. For qRT–PCR, complementary DNA was synthesized and analysed using an ABI light cycler. For analysis of cell death, embryos were stained with LysoTracker Red (Invitrogen) and sectioned. For each section, the LysoTracker-Red-positive and limb bud areas were measured using tools in Adobe Photoshop. The *Meis1*-negative domain was determined for each sample by four independent, blind measurements that were then averaged.

Full Methods and any associated references are available in the online version of the paper at www.nature.com/nature.

Received 28 November 2007; accepted 22 February 2008.
Published online 30 April 2008.

1. Mariani, F. V. & Martin, G. R. Deciphering skeletal patterning: clues from the limb. *Nature* **423,** 319–325 (2003).
2. Tabin, C. & Wolpert, L. Rethinking the proximodistal axis of the vertebrate limb in the molecular era. *Genes Dev.* **21,** 1433–1442 (2007).
3. Niswander, L., Tickle, C., Vogel, A., Booth, I. & Martin, G. R. FGF-4 replaces the apical ectodermal ridge and directs outgrowth and patterning of the limb. *Cell* **75,** 579–587 (1993).
4. Fallon, J. F. *et al.* FGF-2: apical ectodermal ridge growth signal for chick limb development. *Science* **264,** 104–107 (1994).
5. Sun, X. *et al.* Conditional inactivation of *Fgf4* reveals complexity of signalling during limb bud development. *Nature Genet.* **25,** 83–86 (2000).
6. Lewandoski, M., Sun, X. & Martin, G. R. Fgf8 signalling from the AER is essential for normal limb development. *Nature Genet.* **26,** 460–463 (2000).
7. Moon, A. M. & Capecchi, M. R. Fgf8 is required for outgrowth and patterning of the limbs. *Nature Genet.* **26,** 455–459 (2000).
8. Crossley, P. H. & Martin, G. R. The mouse *Fgf8* gene encodes a family of polypeptides and is expressed in regions that direct outgrowth and patterning in the developing embryo. *Development* **121,** 439–451 (1995).
9. Moon, A. M., Boulet, A. M. & Capecchi, M. R. Normal limb development in conditional mutants of Fgf4. *Development* **127,** 989–996 (2000).
10. Colvin, J. S., White, A. C., Pratt, S. J. & Ornitz, D. M. Lung hypoplasia and neonatal death in *Fgf9*-null mice identify this gene as an essential regulator of lung mesenchyme. *Development* **128,** 2095–2106 (2001).
11. Xu, J., Liu, Z. & Ornitz, D. M. Temporal and spatial gradients of Fgf8 and Fgf17 regulate proliferation and differentiation of midline cerebellar structures. *Development* **127,** 1833–1843 (2000).
12. Laufer, E., Nelson, C. E., Johnson, R. L., Morgan, B. A. & Tabin, C. *Sonic hedgehog* and *Fgf-4* act through a signaling cascade and feedback loop to integrate growth and patterning of the developing limb bud. *Cell* **79,** 993–1003 (1994).
13. Niswander, L., Jeffrey, S., Martin, G. R. & Tickle, C. A positive feedback loop coordinates growth and patterning in the vertebrate limb. *Nature* **371,** 609–612 (1994).
14. Sun, X., Mariani, F. V. & Martin, G. R. Functions of FGF signalling from the apical ectodermal ridge in limb development. *Nature* **418,** 501–508 (2002).
15. Boulet, A. M., Moon, A. M., Arenkiel, B. R. & Capecchi, M. R. The roles of Fgf4 and Fgf8 in limb bud initiation and outgrowth. *Dev. Biol.* **273,** 361–372 (2004).
16. Wright, E. *et al.* The *Sry*-related gene *Sox9* is expressed during chondrogenesis in mouse embryos. *Nature Genet.* **9,** 15–20 (1995).
17. Lu, P., Minowada, G. & Martin, G. R. Increasing *Fgf4* expression in the mouse limb bud causes polysyndactyly and rescues the skeletal defects that result from loss of *Fgf8* function. *Development* **133,** 33–42 (2006).
18. Kawakami, Y. *et al.* MKP3 mediates the cellular response to FGF8 signalling in the vertebrate limb. *Nature Cell Biol.* **5,** 513–519 (2003).
19. Sato, K., Koizumi, Y., Takahashi, M., Kuroiwa, A. & Tamura, K. Specification of cell fate along the proximal–distal axis in the developing chick limb bud. *Development* **134,** 1397–1406 (2007).
20. Mercader, N. *et al.* Conserved regulation of proximodistal limb axis development by Meis1/Hth. *Nature* **402,** 425–429 (1999).
21. Mercader, N. *et al.* Opposing RA and FGF signals control proximodistal vertebrate limb development through regulation of Meis genes. *Development* **127,** 3961–3970 (2000).
22. Summerbell, D., Lewis, J. H. & Wolpert, L. Positional information in chick limb morphogenesis. *Nature* **244,** 492–496 (1973).
23. Dudley, A. T., Ros, M. A. & Tabin, C. J. A re-examination of proximodistal patterning during vertebrate limb development. *Nature* **418,** 539–544 (2002).
24. Maden, M. Intercalary regeneration in the amphibian limb and the rule of distal transformation. *J. Embryol. Exp. Morphol.* **56,** 201–209 (1980).
25. Stocum, D. L. The urodele limb regeneration blastema. Determination and organization of the morphogenetic field. *Differentiation* **27,** 13–28 (1984).
26. Wolpert, L., Tickle, C. & Sampford, M. The effect of cell killing by x-irradiation on pattern formation in the chick limb. *J. Embryol. Exp. Morphol.* **50,** 175–193 (1979).
27. Barna, M. & Niswander, L. Visualization of cartilage formation: insight into cellular properties of skeletal progenitors and chondrodysplasia syndromes. *Dev. Cell* **12,** 931–941 (2007).
28. Pajni-Underwood, S., Wilson, C. P., Elder, C., Mishina, Y. & Lewandoski, M. BMP signals control limb bud interdigital programmed cell death by regulating FGF signaling. *Development* **134,** 2359–2368 (2007).
29. Hung, I. H., Yu, K., Lavine, K. J. & Ornitz, D. M. FGF9 regulates early hypertrophic chondrocyte differentiation and skeletal vascularization in the developing stylopod. *Dev. Biol.* **307,** 300–313 (2007).
30. Zucker, R. M., Hunter, E. S. III & Rogers, J. M. Apoptosis and morphology in mouse embryos by confocal laser scanning microscopy. *Methods* **18,** 473–480 (1999).

Supplementary Information is linked to the online version of the paper at www.nature.com/nature.

Acknowledgements We thank D. Ornitz for providing mice carrying the *Fgf9* and *Fgf17* null alleles before publication, and D. Lakeland for help with the statistical analysis. We are grateful to P. Ghatpande, A. Nemati and E. Yu for technical assistance. We also thank M. Barna, X. Sun, R. Metzger and our laboratory colleagues for comments on the manuscript. F.M. was supported by a fellowship from the American Heart Association and a National Research Service Award (NIH). This work was supported by a grant from the National Institutes of Health (R01 HD34380) to G.R.M.

Author Information Reprints and permissions information is available at www.nature.com/reprints. Correspondence and requests for materials should be addressed to G.R.M. (gail.r.martin@ucsf.edu).

METHODS

Production and analysis of mice. Strategies similar to that used for generating the F4;9,17-TKO mutants (Fig. 1b) were used to generate animals of the other genotypes used in this study. For example, to generate F8;9-DKO or F8-KO;F9$^{+/-}$ offspring, *Msx2-cre*,*Fgf9*$^{-/+}$;*Fgf8*$^{\Delta 2,3/fl}$ males were crossed with *Fgf9*$^{-/+}$;*Fgf8*$^{fl/fl}$ or *Fgf8*$^{fl/fl}$ females. F4;8;9-TKO or F4;8-DKO;F9$^{-/+}$ animals were generated by crossing *Msx2-cre*,*Fgf9*$^{-/+}$;*Fgf4*$^{\Delta 2,3/fl}$;*Fgf8*$^{fl/fl}$ males with *Fgf9*$^{-/+}$;*Fgf4*$^{fl/fl}$;*Fgf8*$^{fl/fl}$ or *Fgf4*$^{fl/fl}$;*Fgf8*$^{fl/fl}$ females. F8-KO and F8;F4-DKO animals were generated as previously described[6,14]. Animals were genotyped by PCR on DNA isolated from head or tail tissue, using primer pairs for *Msx2-cre*, *Fgf4* and *Fgf8* alleles[14]. For *Fgf9*, we used the following primers: wild-type allele forward, 5′-GCAAGGGAGGGGAGTTGGATATACC-3′, and reverse, 5′-GAAATCCAGTCCTGCAGTACAGCTGC-3′; mutant allele forward, 5′-CCTTTTTCCCTCTCTGTCTGCAAC-3′, and reverse, 5′-TGTGCTCTAGTAGCTTTACGGAGCC-3′. For *Fgf17*, the primers were: wild-type allele forward, 5′-GAAGTTTCTCCAGCGATGGG-3′, and reverse, 5′-GACAGCAGAGAATCAATAGCTGC-3′; mutant allele forward, 5′-CCATGAGTGAACGAACCTGG-3′,and reverse, 5′-TTGGCTTCTCTGGGACTCTACC-3′. Because homozygosity for *Fgf9* function causes perinatal lethality[10], we assayed for skeletal pattern at E17.5 by staining cartilage and bone with alcian blue and alizarin red, respectively, using standard procedures. Embryos younger than E11 were staged by counting somites as described previously[5]. Whole-mount RNA *in situ* hybridization was performed according to a standard protocol.

Limb bud analysis. Limbs for qRT–PCR were dissected and stored at –20 °C in RNAlater (Qiagen, catalogue number 1017980) until genotyping information was obtained. Individual limbs were then homogenized with the rotor-stator method and RNA was extracted (RNeasy micro kit, Qiagen, catalogue number 74004, including the DNase I step). Complementary DNA was then synthesized (High Capacity cDNA kit, Applied Biosystems, catalogue number 4368814) and analysed with an ABI light cycler with the following primers: cyclophilin forward, 5′-TGGAGAGCACCAAGACAGACA-3′, and reverse, 5′-TGCCGGAGTCGACAATGAT-3′; *Fgf8* forward, 5′-TCTCCAGCACGATCTCTGTGAA-3′, and reverse, 5′-GGAAGCTAATTGCCAAGAGCAA-3′; *Shh* forward, 5′-AGCAGACCGGCTGATGACT-3′, and reverse, 5′-AGAGATGGCCAAGGCATTTAA-3′. No-template controls and reverse transcriptase negative controls were included to detect contaminating genomic DNA. In addition, we performed control experiments in which we made cDNA from 0.5, 1, 2 and 4 limb buds to confirm that we could detect small differences in *Fgf8* and *Shh* expression.

Limb buds from embryos stained with LysoTracker Red as previously described[31], were embedded in 4% low-melt agarose and sectioned (25 μm) on a Leica vibrating microtome. Serial transverse sections were collected, counterstained with 4,6-diamidino-2-phenylindole (DAPI), mounted on slides, and photographed on a Zeiss Axiophot fluorescence microscope or a Nikon Spectral confocal microscope at the UCSF Nikon Imaging Center. For each section, the LysoTracker-Red-positive area was measured by setting a black/white threshold level in the image of the limb bud in that section and counting white pixels in the mesenchyme. The area was measured by counting the total number of pixels in the image of the limb bud. Data from each section were summed across the sample (voxels) to obtain the total amount of cell death and the size (volume) of each limb bud.

31. Grieshammer, U. *et al.* FGF8 is required for cell survival at distinct stages of nephrogenesis and for regulation of gene expression in nascent nephrons. *Development* **132**, 3847–3857 (2005).